The Astrophysical Journal, 805:71 (9pp), 2015 May 20 doi:10.1088/0004-637X/805/1/71

DETECTION OF A LIGHT ECHO FROM THE OTHERWISE NORMAL SN 2007af

D. Drozdov[1], M. D. Leising[1], P. A. Milne[2], J. Pearcy[2], A. G. Riess[3], L. M. Macri[4], G. L. Bryngelson[5], and P. M. Garnavich[6]
[1] Department of Physics and Astronomy, Clemson University, Clemson, SC 29634, USA
[2] University of Arizona, Steward Observatory, Tucson, AZ 85719, USA
[3] Department of Physics and Astronomy, Johns Hopkins University, Baltimore, MD 21218, USA
[4] George P. and Cynthia Woods Mitchell Institute for Fundamental Physics and Astronomy, Department of Physics & Astronomy, Texas A&M University, 4242 TAMU, College Station, TX 77843, USA
[5] Department of Physics and Astronomy, Francis Marion University, Florence, SC 29501, USA
[6] Physics Department, University of Notre Dame, Notre Dame, IN 45556, USA
Received 2014 October 27; accepted 2015 March 4; published 2015 May 21

ABSTRACT

We present the discovery of a light echo from SN 2007af, a normal Type Ia supernova (SN Ia) in NGC 5584. *Hubble Space Telescope* images taken three years post explosion reveal two separate echoes: an outer echo and an extended central region, which we propose to be an inner echo for which details are unresolved. Multiple images were obtained in the F160W, F350LP, F555W, and F814W using the Wide Field Camera 3. If the outer echo is produced by an interstellar dust sheet perpendicular to the line of sight, it is located ~800 pc in front of the SN. The dust for the inner echo is 0.45 pc $< d <$ 90 pc away from the SN. The inner echo color is consistent with typical interstellar dust wavelength-dependent scattering cross-sections, while the outer echo is redder than predicted. Both dust sheets, if in the foreground, are optically thin for scattering, and the outer echo sheet thickness is consistent with the inferred extinction from peak brightness. Whether the inner echo is from interstellar or circumstellar dust is ambiguous. Overall, the echo characteristics are quite similar to previously observed SN Ia echoes.

Key words: circumstellar matter – dust, extinction – galaxies: individual (NGC 5584) – supernovae: general – supernovae: individual (SN 2007af)

1. INTRODUCTION

Type Ia supernovae (SNe Ia) have long been invoked as "standard candle" distance indicators due to their extreme luminosity and relative homogeneity of that luminosity. Although powerful as tools in astronomy, there are fundamental properties of the underlying physics that are not yet fully understood. Single-degenerate (SD) and double-degenerate (DD) progenitor binary systems have been proposed to produce SNe Ia, and various explosion models have been suggested to describe these seemingly uniform objects. Among the approaches to discern new information about supernovae and their environments, light echoes (LEs) can be effective probes of both the circumstellar and interstellar environments.

Detectable LEs are rare events, where the light from a bright source scatters off surrounding dust and reaches the observer after a delay caused by the extra distance traveled. Evidence of LEs were first discovered from Nova Persei 1901 (Ritchey 1901a, 1901b, 1902). Since that time, LEs have been seen from Galactic Nova Sagittarii (Swope 1940), Galactic Cepheid RS Puppis (Havlen 1972), V838 Monocerotis (Bond et al. 2003), young stars (Ortiz et al. 2010), and other phenomena (see Sugerman 2003). Some examples from core-collapse supernovae include the very nearby case of SN 1987 A (Crotts 1988; Gouiffes et al. 1988; Suntzeff et al. 1988; Panagia et al. 1991), SN 1993 J (Liu et al. 2003), SN 1999ev (van Dyk et al. 2003; Maund & Smartt 2005), SN 2003gd (Sugerman 2005), SN 1980 K (Sugerman et al. 2012), SN 2004et (Otsuka et al. 2012), SN 2005at (Kankare et al. 2014), SN 2006gy (Miller et al. 2010), and SN 2008bk (van Dyk 2013).

Light echoes can be used to determine various dust properties of the host galaxy (Patat 2005). Time-variability of spectral features near peak brightness suggests the presence of circumstellar material (CSM). The CSM could be due to stellar winds and/or non-conservative mass transfer from the donor star. The presence of CSM has often been treated as evidence of a single degenerate progenitor system, but recent studies suggest that both SD and DD scenarios can produce CSM (Moore & Bildsten 2012; Shen et al. 2012; Raskin & Kasen 2013). The mass-loss history and the progenitor system can be investigated from the detection of a CSM light echo.

The SN-dust distance can be found simply from the geometry of an interstellar echo. Because they reveal the dusty nature of the surroundings, LEs can also be used to probe the suggested association of some SNe Ia with star-forming regions, and, therefore, the young nature of the progenitors (Howell 2001). The distance to the host galaxy can be determined geometrically from the ring of maximum linear polarization from echoes (Sparks 1994). In practice, this method is limited by the point-spread function (PSF) of the image.

Light echoes have also been used to classify historical SNe (Krause et al. 2008; Rest et al. 2008). Light echoes are dominated by scattered peak light, and the light-curve weighted mean of the spectrum can be compared to standard SNe spectra for classification purposes. Understanding the prevalence and characteristics of LEs is essential for late-time monitoring of SN Ia power since weak echoes might be misinterpreted (e.g., as dissipation of trapped positron kinetic energy, when the light curve falls 10 or more magnitudes below peak brightness). Since echoes are most easily detected after the SN emission has diminished, the small sample of detectable LEs from SNe Ia could be due to the lack of late-time observations.

Five SN Ia LEs have been reported to date (SN 1991 T (Schmidt et al. 1994), SN 1998bu (Cappellaro et al. 2001;

Garnavich et al. 2001), SN 1995 E (Quinn et al. 2006), SN 2006X (Crotts & Yourdon 2008; Wang et al. 2008), and SN 2014 J (Crotts 2014)). Here we report the detection of a light echo from SN 2007af discovered in *Hubble Space Telescope* (*HST*) images and corroborated with ground-based observations. The paper is organized as follows. Early- and late-epoch observations of SN 2007af are discussed in Section 2. The light echo analyses and interpretations are located in Sections 3 and 4, respectively. Section 5 focuses on the interstellar versus circumstellar dust argument for the inner echo creation, and we present our conclusions in Section 6.

2. SN 2007AF

SN 2007af was discovered by K. Itagaki on 2007 March 1.84 (UT dates are used throughout) at $\alpha = 14^{h}\,22^{m}\,21\overset{s}{.}03$, and $\delta = -0^{\circ}\,23'\,37\overset{''}{.}6$ well before maximum. The location of the SN was offset 40″ west and 22″ south from the dusty center of the host galaxy, NGC 5584. NGC 5584 is an Scd galaxy with a recession velocity of $1638\,\mathrm{km\,s^{-1}}$ (Koribalski et al. 2004). SN 2007af was classified as a normal SN Ia by its spectrum taken on 2007 March 4.34 (Salgado et al. 2007).

Simon et al. (2007) reported on the lack of time-variability of the Na D absorption features in the spectra of SN 2007af, in contrast to the variability observed from SN 2006X by Patat et al. (2007). High-resolution spectra were taken at −4.3, +16.6, and +23.7 days relative to maximum light using the ARCES echelle spectrograph on the ARC 3.5 m telescope at the Apache Point Observatory. Na D absorption lines and the Hα emission line were extensively investigated, but no variability was detected. Due to the lack of variation in the spectral absorption features, the authors conclude that absorbing gas from the interstellar medium of NGC 5584 is responsible for the Na D absorption lines. The progenitor system either differs from the SD circumstellar case of SN 2006X or spectroscopic variability is not detectable along all viewing directions. The lack of time-variability constrains the location of the CSM, but does not rule out its existence.

The line-of-sight extinction estimate from Simon et al. (2007) was $A_V = 0.39 \pm 0.06$ mag using an extinction law of $R_V = 2.98 \pm 0.33$. Due to the low extinction and the normal behavior at peak, SN 2007af was considered an unlikely candidate for a light echo.

SN 2007af was the target of multiple photometric campaigns due to its pre-maximum discovery. Ultraviolet, near-infrared, and optical photometry were performed on this normal SN Ia by a variety of teams and telescopes. The separation of the SN from the center of the host galaxy and the relatively nearby galaxy provided an ideal SN for intensive study.

2.1. Steward Observations

We monitored SN 2007af with the Montreal 4 K imager on the 1.5 m Kuiper telescope and the 90Prime Imager on the 2.3 m Bok telescope. The 61″ Kuiper telescope is located on Mount Bigelow in the Santa Catalina Mountains. The optical imager is equipped with a Fairchild 4000 × 4000 CCD with a 9.′7 × 9.′7 field of view. The telescope features a primary focal ratio of *f*/13.5 Cassegrain focus. The optical imager used on the Bok telescope on Kitt Peak, 90Prime, is a prime focus, wide-field imager, which utilizes a mosaic array of four 4000 × 4000 pixel CCDs and images an area of 1.0 square degrees. Aperture photometry was performed using Landolt standard stars (Landolt 1992), and the images were reduced using standard IRAF[7] procedures. The late-epoch Steward observations were analyzed after template subtraction using both *HST* images and images obtained from the NASA/IPAC Extragalactic Database (NED).[8]

2.2. HST Observations

To use high-redshift SNe Ia in cosmology, the absolute magnitudes of SNe Ia must be calibrated. The best calibrations of SNe Ia use Cepheid variable stars in the host galaxies of low-redshift SNe Ia, which are calibrated with parallax and main-sequence fitting, two nearby rungs of the distance ladder. Cepheid variable monitoring is one of the techniques used to measure the H_o, the present expansion rate of the universe. The "Supernovae and H_o for the Equation of State" (SHOES) project aimed to measure the expansion rate to < 5% precision using SNe Ia and Cepheids. The SNe Ia chosen for this cosmological study had to fit the following criteria: available modern photometric data (e.g., CCD) and observations before the peak, low reddening ($A_V < 0.5$ mag), spectroscopically classified as normal, and have *HST* optical observations of Cepheid variables in the SN host galaxy (Riess et al. 2011).

NGC 5584 was discovered to have a wealth of Cepheids and was observed with the Wide Field Camera 3 (WFC3) during *HST* Cycle 17 as part of *HST* program 11570: P.I. A. Riess. NGC 5584 was observed in the F160W (wide *H*), F350LP (unfiltered long pass), F555W (wide *V*), and F814W (wide *I*) filters from 2010 January to April, 3 yr after the explosion of the SN. The individual exposures were 400–700 s in length with a total exposure time equaling 4926 s. Integer and half-pixel dithering were enabled between exposures to characterize the PSF.

2.3. Light Curve

Early- and late-epoch observations complete the light curve (Figure 1) and are plotted against the dashed line of normal Type Ia SN 1992 A (Suntzeff et al. 1996). At early epochs, the light curve shows no deviation from the normal template, and since little dust was detected at peak along the line of sight, this SN was considered a poor candidate for an echo. The normal peak behavior of SN 2007af is in sharp contrast to the late plateau. The 2009 March 18.2 (JD = 2454908.5) observations, two years past explosion, show that this SN has declined considerably less than SN 1992 A at a comparable epoch. The emission from SN 1992 A during that epoch is thought to be due to the energy deposition from positrons created in $^{56}\mathrm{Co} \rightarrow {}^{56}\mathrm{Fe}$ decays (Suntzeff et al. 1996; Milne et. al., 1999). The obvious flattening of the SN 2007af light curve compared to the decline rate from intrinsic emission is attributed to the existence of a light echo. Patat (2005) has argued that LEs should be 10–12 magnitudes fainter than the SN at peak, which is consistent with the observational sample. A light echo 10 magnitudes fainter than peak will reveal itself at 450+ days post-maximum.

[7] The Image Reduction and Analysis Facility (IRAF) is publicly distributed by the National Optical Astronomy Observatory (NOAO) in Tucson, AZ. NOAO is operated by the Association of Universities for Research in Astronomy, Inc., in cooperation with the National Science Foundation.

[8] The NASA/IPAC Extragalactic Database (NED) is operated by the Jet Propulsion Laboratory, California Institute of Technology, under contract with the National Aeronautics and Space Administration.

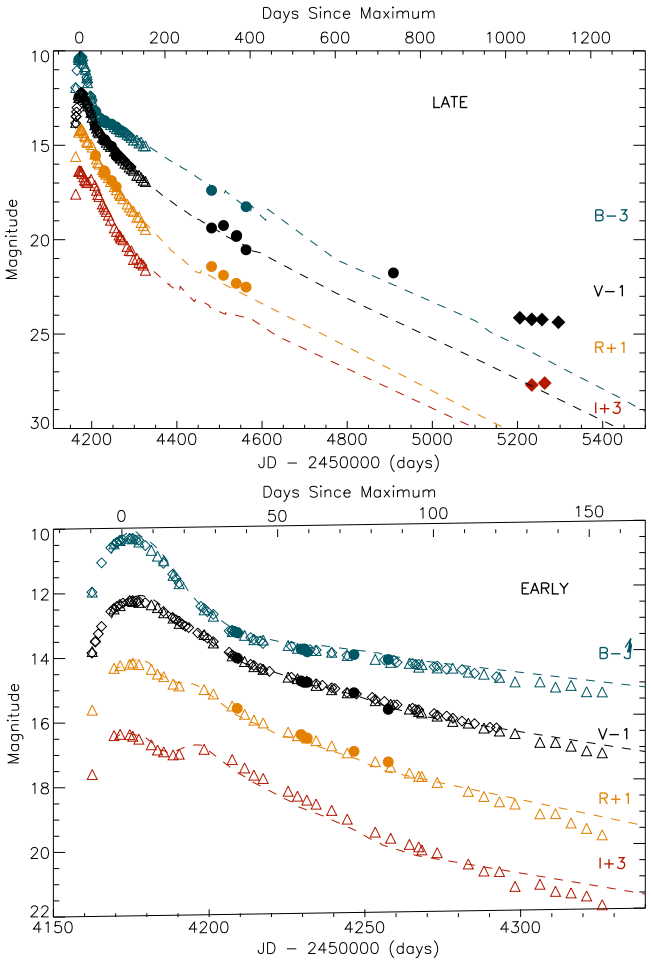

Figure 1. Early (lower panel) and complete (upper panel) *BVRI* light curves of SN 2007af plotted against normal SN 1992 A (dashed line; Suntzeff et al. 1996). The light echo dominates at late times. The *HST* images are labeled with black diamonds (F555W) and red diamonds (F814W). Steward observations are distinguished with filled circles. The early data was taken from CfA3 (*BV*-open diamonds) and KAIT (*BVRI*-open triangles; Hicken et al. 2009; Simon et al. 2007).

The distinct flattening is present in *V* and *I*, suggesting that an echo was captured in both the *HST* images and ground-based Steward Observatory late-epoch observations in *V*. SN 2007af was well observed in the transition from intrinsic to light echo emission. At over 1000 days after peak, the SN is ∼4 magnitudes brighter than predicted from intrinsic emission.

3. LIGHT ECHO IMAGING

The *HST* images reveal the light echo visually (Figure 2). These ∼1000 days post explosion images show a ring-like object and extended central source at the location of the SN, which we call the outer and inner LEs.

The Cepheid campaign began in 2010 January, 2.8 yr after the SN peak brightness. Thirty-nine images were stacked to improve the signal-to-noise ratio in four filters, with the LEs detected in all but the F160W(*IR*) filter. The echoes are clearly weaker in the F814W filter than in F350LP and F555W. The echoes are faint, and, in particular, the surface brightness of the outer feature is very low. The region contains a number of other emission features, both stellar and otherwise. We characterized

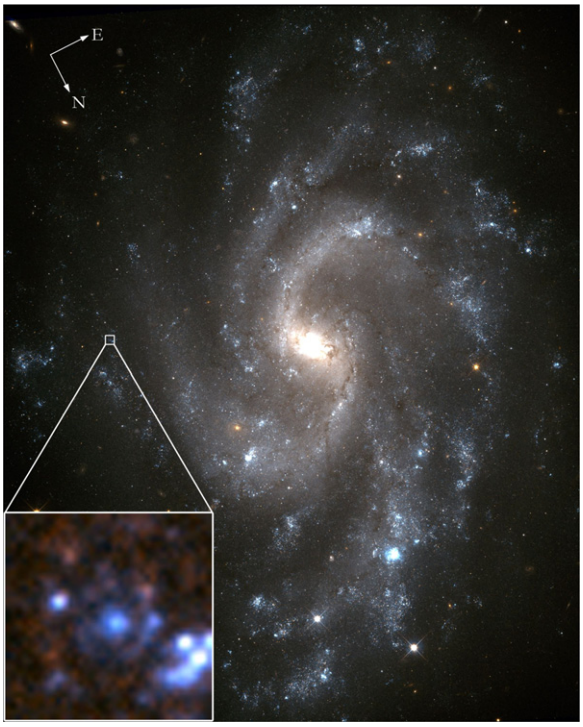

Figure 2. Color composite image of NGC 5584 and the combined light echo image of SN 2007af (inset panel) from *HST* WFC3. The SN location (box) is shown in NGC 5584, and the 2″ × 2″ close up of the region shows both echoes in the center of the box, nestled in between the white stellar source on the middle left and the group of white sources on the bottom right. The images are the result of stacking the individual monthly observations in all filters. A ring (outer echo) surrounds the bright central region, which we propose to be a secondary light echo (inner echo).

the echoes by fitting defined shapes convolved with the PSF's of the images (see Figure 3).

In this analysis, we select a limited region around the SN location, determine the PSF size from a number of stars (typically twenty), subtract stellar objects near the SN, and perform non-linear least-squares fits of two shapes plus background to a region typically twenty-five pixels square around the SN. The PSF's are assumed to be azimuthally symmetric radial Gaussians and are found to be consistent with 0.″11 FWHM. We tried a variety of different shapes for the echo features. Fits of elliptical functions did not yield significant eccentricity, regardless of axis orientations, so we only quote fits for azimuthally symmetric functions. For the central source, we tried a flat plateau and exponentials, but no shape fits significantly better than a two-dimensional radial Gaussian, therefore, we use that. For the outer annular echo, we use a radial function that falls off as a Gaussian from a radius of maximum.

Our general fit has 10 parameters: a constant background, central Gaussian amplitude and width, Gaussian annulus amplitude, peak radius and width, and two coordinates of the center of each of the echo shapes. Convergence is unpredictable with all parameters free because of correlations among them, so we generally constrain some of them. If we try to determine the locations of the centroids of the echoes by fixing the widths of the two echoes, we always find the coordinates of both echo centers are consistent with the location of the SN and with each other, strengthening the argument of two separate echo detections. The locations are within one-half pixel of the

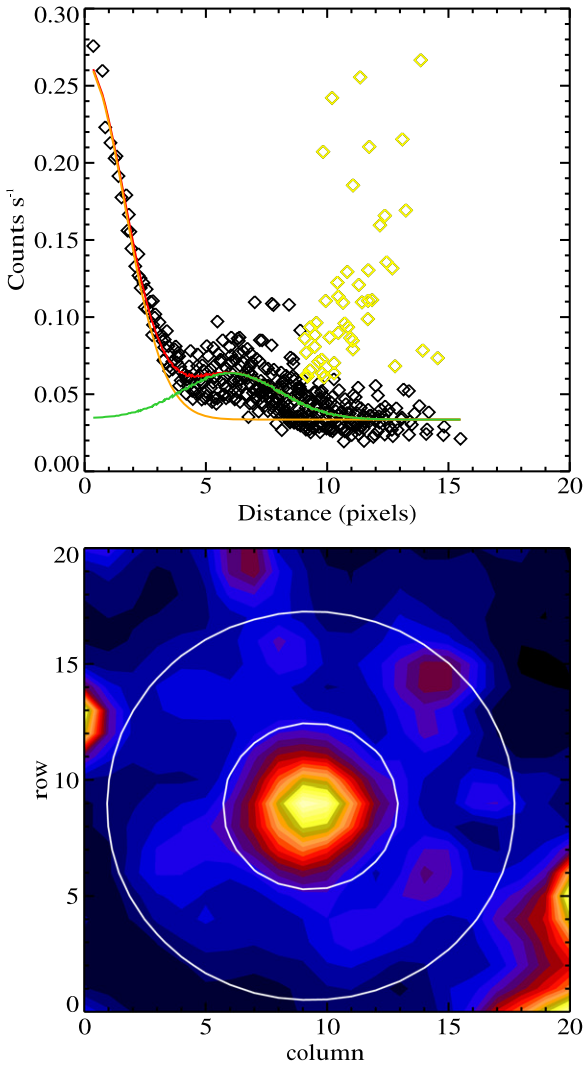

Figure 3. Example of the fit of our echoes in the F350LP band. The top panel shows the count contributions in our crowded field. The yellow diamonds are high points outside the outer echo that have been omitted from the field, the green line is the outer echo contribution, the orange line is the inner echo contribution, and red represents the inner and outer echo combined. The bottom panel shows both echoes, where the white circles are 50% contours of the outer echo. The axes for the top panel are counts versus distance in pixels from the centers of the two echoes, and the bottom panel's axes are pixel numbers from an arbitrary point on the CCD.

Table 1
Optical Photometry from the Steward Observatory

JD (days)	B	err(B)	V	err(V)	R	err(R)
2454208.9	16.199	0.004	14.985	0.001	14.543	0.002
2454229.5	16.709	0.004	15.694	0.002	15.352	0.002
2454230.5	16.702	0.004	15.737	0.003	15.443	0.002
2454231.5	16.792	0.004	15.734	0.002	15.461	0.002
2454246.5	16.878	0.004	16.059	0.002	15.872	0.004
2454257.5	17.030	0.007	16.573	0.007	16.200	0.003
2454481.5	20.390	0.048	20.381	0.040	20.422	0.407
2454509.5	...	...	20.250	0.040	20.888	0.070
2454539.5	...	...	20.830	0.065	21.315	0.081
2454540.5	...	...	20.780	0.030	...	...
2454562.5	21.253	0.068	21.537	0.076	21.514	0.080
2454908.5	...	...	22.762	0.462	...	...

Table 2
Angular Sizes of Echoes

Filter	JD (days)	$\theta_{\rm OE}$ (″)	$\theta_{\rm IE}$ (″)
F350LP	2455205.43	0.34 ± 0.01	0.13 ± 0.02
F350LP	2455233.52	0.32 ± 0.01	0.10 ± 0.02
F350LP	2455257.48	0.33 ± 0.01	0.11 ± 0.02
F350LP	2455296.04	0.33 ± 0.01	0.13 ± 0.02
F555W	2455205.35	0.32 ± 0.01	0.12 ± 0.02
F555W	2455233.44	0.31 ± 0.01	0.11 ± 0.02
F555W	2455244.37	0.32 ± 0.01	0.11 ± 0.02
F555W	2455257.35	0.32 ± 0.01	0.10 ± 0.01
F555W	2455295.96	0.32 ± 0.01	0.11 ± 0.02
F814W	2455233.57	0.35 ± 0.01	0.09 ± 0.03
F814W	2455263.82	0.32 ± 0.01	0.08 ± 0.03

SN position with a one-sigma uncertainty of typically 0.2 pixels using the world coordinate system coordinates of the echo centers in the *HST* images compared to the coordinates of the SN position. To determine the intensities and widths of the features, we constrain the coordinates of the centers of the two to be the same for both. Also, the two widths and the annulus radius are highly correlated for our quoted sizes and fluxes, so we fix the annulus FWHM at the mean best-fit value (0.″16) and allow the central source FWHM and annulus peak radius to vary.

Where there are non-stellar features in the fit region that are unrelated to the SN echoes, we exclude those points from the fits. The models are convolved with the PSF's and fit to the data. The resulting least-squares fits are typically not formally good fits, with reduced χ^2 that is typically 1.5–2.0 for 450 degrees of freedom. The central echo is generally well fit, but the outer echo is not smooth and not very well fit by a smooth azimuthally symmetric echo. Still, the fits capture the sizes and brightnesses of the echo components well. The intrinsic angular radii measurements for the outer ($\theta_{\rm OE}$) and inner echoes ($\theta_{\rm IE}$) can be found in Table 2 for each filter.

Light echo rings should grow with time if produced by a continuous dust sheet scattering the light. Unfortunately, the four month timespan combined with the uncertainty in the angular size of both echoes results in a growth beneath our resolving capability. To confirm the growth of both echoes, subsequent imaging would be necessary.

To independently confirm the extent of the central echo, the FWHM of the source was determined using the radial profile task (r mode, which uses a radial profile Gaussian fit) in IMEXAMINE in IRAF (Tody 1986). This analysis was successful on all echo images but F814W, exhibiting the same trend in each. The fit did not converge in the F814W filter due to the weaker signal, and only an estimation could be obtained. The average FWHM of the local stars was 2.63 ± 0.4 pixels compared to the average inner echo FWHM of 4.03 ± 0.3 pixels. Thus, the inner echo has an FWHM that is extended 1.53 times relative to the local stars in the field. This test illustrates the broadened feature of the source and definitively refutes the notion that the central component is simply a background star. The broadening can be interpreted as nebulosity caused by a light echo, but an extended non-echo source cannot be eliminated.

Table 3
Light Echo Magnitudes[a]

Filter	JD (days)	$\text{Magnitude}_{\text{OE}}$	$\text{Magnitude}_{\text{IE}}$	$\text{Magnitude}_{\text{Total}}$
F350LP	2455205.43	24.477 ± 0.065	25.202 ± 0.199	24.028
F350LP	2455233.52	24.611 ± 0.066	25.369 ± 0.188	24.173
F350LP	2455257.48	24.552 ± 0.066	25.327 ± 0.189	24.119
F350LP	2455296.04	24.832 ± 0.085	25.337 ± 0.217	24.303
F555W	2455205.35	24.511 ± 0.057	25.109 ± 0.171	24.017
F555W	2455233.44	24.591 ± 0.072	25.204 ± 0.199	24.103
F555W	2455244.37	24.600 ± 0.064	25.223 ± 0.180	24.115
F555W	2455257.35	24.575 ± 0.063	25.259 ± 0.167	24.111
F555W	2455295.96	24.832 ± 0.084	25.213 ± 0.182	24.253
F814W	2455233.57	25.058 ± 0.158	25.962 ± 0.374	24.666
F814W	2455263.82	24.819 ± 0.119	26.250 ± 0.452	24.562

[a] All magnitudes listed are in VEGA magnitudes.

3.1. Light Echo Magnitude

Light echo magnitudes were determined using the fits mentioned previously and are consistent with the values obtained by estimating by eye the sizes of circular apertures and summing the counts enclosed.

The counts were converted to VEGA magnitudes using the WFC3 header keyword PHOTFLAM, the mean flux density that produces one count per second in observing mode, and the filter zero points provided.[9] The PHOTFLAM values used in our conversions were 5.297E-20 for F350LP, 1.865E-19 for F555W, and 1.514E19 for F814W (in units of erg cm $^{-2}$ s^{-1} Å^{-1}).

The magnitudes of the inner and outer echoes listed by filter and date are listed in Table 3. The total magnitude of the echoes was used in plotting the *HST* observations on the light curve of SN 2007af (Figure 1) since the ground-based observations would not resolve two separate components.

The magnitude difference between the inner and outer echoes changes with filter. For the F350LP filter, there is a ~0.6 mag difference between the outer and inner echo values and ~0.7 mag difference in the F555W filter. For the F814W band, this value increases to ~1.0 mag. Even with the lower sensitivity in the wide*I* filter, this noticeable change suggests a change in dust reflecting properties. This behavior seems inconsistent for two LEs created in the same manner, which could imply a different mechanism for producing the inner echo.

4. PHYSICAL MODEL

Light echoes are effective probes of the surrounding material and simple applications yield ample information about the source. From the geometry of the echoes, a distance between the scattering medium and SN can be inferred, and the color of the echoes reveals information about the scattering effects and dust properties.

4.1. Dust Distance

Analytical treatment of the light echo phenomenon (see Couderc 1939 for more rigorous derivation) states that a dust sheet intersecting the paraboloid of the constant time delay creates a circular ring echo centered on the source solely dependent on the time (t) since peak light and the distance to the host galaxy (D), assuming a dust sheet perpendicular to the line of sight. The distance the dust sheet lies in front of the SN can be simply determined using Equation (1), where θ is the angular radius of the echo:

$$d \approx \frac{D^2\theta^2 - (ct)^2}{2ct}. \quad (1)$$

The foreground distance between the dust sheet and the SN for the outer echo was determined using a $D = 24$ Mpc for NGC 5584 (Simon et al. 2007). For comparison, the distance estimate based on a joint analysis of the Cepheid and SN data by Riess et al. (2011) yields $D = 23 \pm 0.7$ Mpc after correction for the revised maser distance to NGC 4258 (Humphreys et al. 2013). The dust sheet distances can be found in Table 4. The average distance from the SN to the dust sheet is 790 ± 60 pc, implying that ISM dust produced the echo.

The inner echo is consistent with both a CSM and ISM sheet and represents the smallest and largest dust distances allowed by the previous analysis. From our analysis, we cannot elimate the CSM geometry possibility. First, the inner echo dust distance was calculated assuming a circumstellar sheet (d_{IECSM}(pc)). Using the proposed solution of backscattered light, a dust sheet located behind the SN exists at a location determined solely by the time delay of the echo. The initial light from the SN traveled outward, scattered off the dust sheet behind the explosion site, and returned back toward the observer. Therefore, half of the time delay determines the distance to the dust sheet. The average inner echo distance from the SN to the sheet is 0.45 ± 0.01 pc in this scenario. Alternatively, the results for the ISM dust sheet scenario are listed in the last column using the same labeling convention. The inner echo SN-foreground dust sheet distance results in an average of 90 ± 20 pc.

A schematic for the dust geometry (not to scale) for the January epoch in the F555W filter can be seen in Figure 4 for a CSM inner echo. Because the distance from the SN to Earth is much greater than the distance between the SN and the dust, we can approximate the geometry of the phenomenon as a paraboloid. The SN is located at the focus of the paraboloid, and the echo rings are created from the intersection between the dust sheet and the paraboloid (Patat 2005). The orange shaded region shows the intersection that results in the outer echo, and the blue shaded region is the intersection causing the inner echo. Figure 5 shows the same epoch, but with an ISM origin for both echoes.

[9] http://www.stsci.edu/hst/wfc3/phot_zp_lbn.

Table 4
Dust Sheet Distances

Filter	JD (days)	d_{OE}(pc)	d_{IECSM}(pc)	d_{IEISM}(pc)
F350LP	2455205.43	891	0.43	130
F555W	2455205.35	790	0.43	110
F555W	2455233.44	721	0.44	90
F350LP	2455233.52	769	0.44	74
F814W	2455233.57	920	0.44	60
F555W	2455244.37	761	0.45	89
F350LP	2455257.48	800	0.46	88
F555W	2455257.35	752	0.46	88
F814W	2455263.82	748	0.46	46
F350LP	2455296.04	772	0.47	119
F555W	2455295.96	726	0.47	85

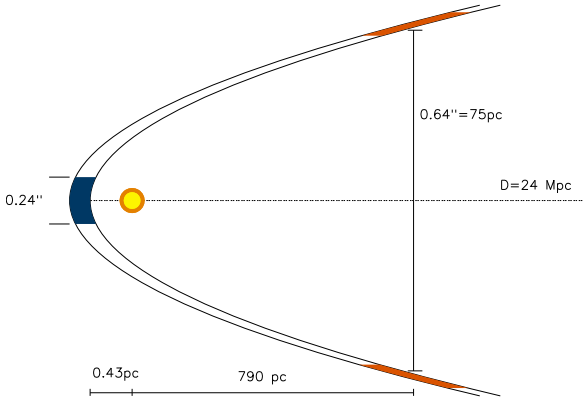

Figure 4. Geometry of the dust that produced the inner echo (blue) and outer light echo (orange) of SN 2007af (not to scale) in the backscattering, CSM scenario. This figure focuses on the January F555W epoch of the light echo, with $\theta_{IE} = 0.''12$, and $\theta_{OE} = 0.''32$. The figure shows the foreground dust sheet for the outer echo and a secondary dust sheet 0.43 pc behind the SN (shown in yellow).

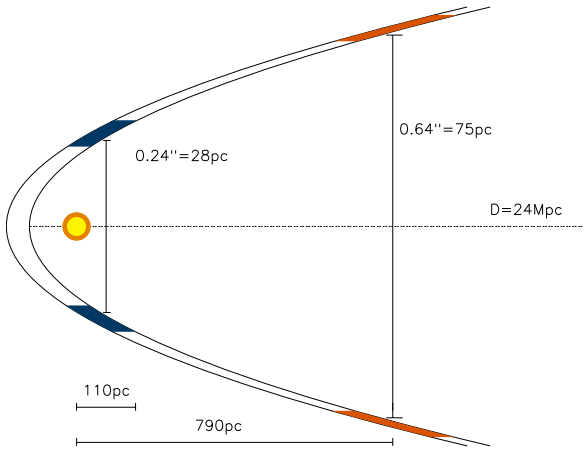

Figure 5. Geometry of the dust that produced the inner echo (blue) and outer light echo (orange) of SN 2007af (not to scale) for the forward scattering, ISM scenario. The outer echo for the January epoch (F555W) was created from a dust sheet 790 pc away from the SN, and the inner echo dust sheet was located 110 pc in front of the SN (shown in yellow).

4.2. Dust Color Analysis

As reported in Simon et al. (2007), SN 2007af peaked on 2007 March 14.76 ± 0.12 days (JD = 2454174.26). Using the Patat (2005) model, the initial light is treated as a flash. The signal received by the observer at a later time (t) is the sum of photons from the SN in the range of time from 0 to t. The global flux measured by the observer is the echo flux combined with the photons that reached the observer on the direct path from the SN, which is then extinction corrected. The light echo flux in a particular passband is given by $F = L_o\, n_o\, C_{scat}\, \Delta t_{SN}\, e^{-\tau_{eff}}\, G(t)$, where L_o is the SN signal, n_o is the number density of scattering particles, and C_{scat} is the scattering cross-section of the dust grains. The flash duration is Δt_{SN}, τ_{eff} is the weighted optical depth for the LE at a given time, and $G(t)$ is a wavelength- and time-dependent function related to the dust geometry.

Table 5
Dust Parameters

Dust Type	Wavelength (Å)	$\theta = 0°$[a] $C_{scat}(cm^2)$	$\theta = 180°$ $C_{scat}(cm^2)$
MW $R_V = 3.1$	5470	1.68E-22	7.30E-24
MW $R_V = 3.1$	8020	6.27E-23	5.88E-24
LMC $R_V = 2.6$	5470	5.32E-23	1.51E-24
LMC $R_V = 2.6$	8020	1.96E-23	1.10E-24
SMC Bar $R_V = 2.9$	5470	2.38E-23	9.81E-25
SMC Bar $R_V = 2.9$	8020	8.85E-24	6.39E-25

[a] $\theta = 0°$ corresponds to forward scattering, and $\theta = 180°$ is backscattering.

The color of the echo from SN 2007af can be predicted using the single scattering approximation model taken from Patat (2005). The predicted color of the echo (Equation (2)) was determined by folding the F555W and F814W WFC3 transmission filters with a peak Branch normal SN Ia spectrum scattered with Draine (2003) dust cross-sections (Nugent et al. 2002) and weighted by the flash duration in each band. These are compared to the Vega spectrum folded with the same filter transmission functions. The observed and theoretical colors are written in terms of F555W–F814W ($V - I$). A normal peak spectrum was used because reddening corrections are then unnecessary, and the peak SN 2007af spectrum did not extend to the blueward wavelengths of the F555W transmission filter. The flash durations were estimated using the peak light curve of SN 2007af. We chose the flash duration to be the number of days, centered around maximum, within one magnitude of the peak value. From Figure 1, the flash durations of V and I were estimated at 0.08 yr (30 days) and 0.11 yr (40 days), respectively. The I band has a longer flash duration due to the second maximum in the light curve. Longer flash durations would lead to thicker echoes in I:

$$(V - I) \approx -2.5 \log \frac{F_V F_I^{Vega}}{F_V^{Vega} F_I}. \quad (2)$$

Some dust parameters used are listed in Table 5 for illustration, where the third column is the scattering cross section for forward scattering ($\theta = 0°$), and the fourth column values are for backward[10] scattering ($\theta = 180°$). C_{scat} corresponds to the differential scattering cross section per H atom, which determines the scattering properties of a particular dust mixture. The values listed are the ones closest to the central wavelength for 555 and 814 W and merely illustrate the relation between forward and backscattering cross section. For our analysis, we integrated over all wavelengths.

[10] ftp://ftp.astro.princeton.edu/draine/dust/mix

Table 6
Comparison between Peak, Echo Color, and Model Predictions

	Observed		Theoretical	
Epoch	$(V-I)$ (mag)	Dust Type	$\theta = 0°$	$\theta = 180°$
Peak	−0.327	MW $R_V = 3.1$	−1.124	−0.291
Outer Echo	-0.317 ± 0.104	LMC $R_V = 2.6$	−1.122	−0.561
Inner Echo	-0.904 ± 0.304	SMC Bar $R_V = 2.9$	−1.127	−0.545

The actual echo colors using the averages measured in each filter was compared to the predicted model colors (Table 6). Also listed is the peak dereddened color of SN 2007af (−0.327 mag), which was obtained by integrating the peak SN spectrum over the filter responses. The results of the Patat (2005) model color for forward and backward scattering calculations for the three dust types are listed in the last two columns. All values listed are in the VEGA magnitude system.

Forward scattering replicates the inner echo color at the far uncertainty limit, but does not distinguish between dust types due to the large uncertainties. However, the outer echo color does not match forward scattering predictions. Backscattering replicates the color of the outer echo, but the angular radius is typical of an echo created from a foreground dust sheet. It is interesting to note that the outer echo color matches the peak measured color, while the inner echo color is bluer than peak. We also tried a secondary method of predicting the echo color by binning the light curve and summing over time bins, with similar results.

Recently, lower R_V values have been reported for SNe Ia. Scattered light (which causes echoes) tends to reduce the ratio of total-to-selective extinction in the optical (Wang 2005). The ratio is significantly lower at longer wavelengths than 3000 Å. Abnormal dust has been cited for adopting a lower R_V value (1.48 ± 0.06) in the case of SN 2006X (Wang et al. 2008). Goobar (2008) published simulations that yielded values from $R_V = 1.5$–2.5, on the basis that lower values originate from the semi-diffusive propagation of the photons near the location of the SN explosion. Eighty SNe Ia were observed with $E(B-V) \leqslant 0.7$ mag. From this study, an average reddening law of $R_V = 1.75 \pm 0.27$ was derived. Focusing on the 69 SNe with color excess, $E(B-V) < 0.25$ mag, produced a total-to-selective ratio value of $R_V \sim 1$, signifying the reddening in SNe Ia may be more complex than previously thought (Nobili & Goobar 2008). The reddening of SN 2007af fits well under both limits, which could explain the difference between the actual color measured and the predictions using higher R_V values. The lowest R_V value used in our analysis, LMC dust, has a predicted color slightly under the upper uncertainty limit in our backscattered scenario. Thus, backscattering could still be a viable solution for the inner echo if using abnormal dust.

4.3. Comparisons

A relation between $E(B-V)$ and Δm, the peak-echo magnitude difference accounting for extinction, can be determined assuming the relationship between scattering and absorption is known. Table 7 lists the values of all reported SNe Ia LEs (except SN 2014J) including SN 2007af (using $R_V = 2.6$). A lower R_V was adopted after the dust analysis results. The combined magnitude for SN 2007af converted to standard Bessell magnitudes was used for this analysis (Bessell 2005). The first three rows were taken from Quinn et al. (2006), and SN 2006X values were reported in Wang et al. (2008). $E(B-V)$ for SN 2007af comes from Simon et al. (2007). The values are plotted in Figure 6, showing the excellent agreement between the SNe and the Patat (2005) model for single and multiple scattering. For low optical depth values ($\tau \leqslant 1.0$), the light echo phenomenon is well described by single scattering. Auto-absorption and attenuation becomes significant for $\tau > 1.0$, and multiple scattering must be considered.

Table 7
SN Ia Light Echo Comparisons

Supernova	$E(B-V)$(mag)	ΔV(mag)
SN 1991T	0.14 ± 0.05	10.73 ± 0.28
SN 1998bu	0.33 ± 0.03	10.26 ± 0.22
SN 1995E	0.74 ± 0.03	10.40 ± 0.22
SN 2006X	1.42 ± 0.04	11.64 ± 0.07
SN 2007af	0.13 ± 0.03	11.38 ± 0.13

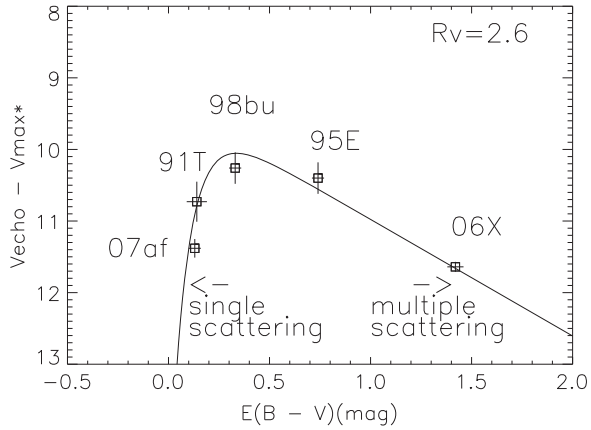

Figure 6. Difference in extinction-corrected V peak to echo magnitude (total magnitude in the case of SN 2007af) compared to the Patat (2005) model for single and multiple scattering using a dust law of $R_V = 2.6$. The figure shows the similarity between the SNe Ia echoes and the excellent agreement to the model.

Patat (2005) proposed that LE luminosity is inversely proportional to SN-dust distance (d) and directly proportional to the optical depth. The peak-to-echo magnitude relationship in the single scattering approximation is shown in Equation (3). The multiple scattering approximation to Δm is given in Equation (4) and follows an exponential decay. These relationships hold for d measured in ly:

$$\Delta m \approx -2.5 \log\left(0.3\frac{\tau}{d}\right) \quad (0 < \tau \leqslant 1), \tag{3}$$

$$\Delta m \approx -2.5 \log\left(\frac{0.3}{d}e^{-\tau}\right) \quad (\tau > 1). \tag{4}$$

Peak magnitude extinction correction was performed using ratios of total-to-selective extinction of $R_V = 2.6 \pm 0.1$ and $R_I = 1.48 \pm 0.1$. The inner echoes have not been extinction corrected because the dust associated with the outer echo would be the dominant cause of the extinction of peak light. The optical depth was calculated using the ISM distances for the inner echo and outer echo. The V optical depths are 0.15 and 0.01 for the outer and inner echoes, respectively. For I, the values are 0.16 and 0.01. From the large dispersion in the values, it is clear that the dust sheet for the inner echo must be optically thin. This confirms the outer echo dust sheet

dominance to the line-of-sight extinction. Because of the low optical depth, SN 2007af fits within the single scattering approximation.

SN 2007af featured a lower $E(B-V)$ at peak than average SNe Ia and the lowest value of all light echo candidates to date. The fact that a significant portion of the sample of SNe Ia found with LEs have low extinction values is surprising. SN 2007af showed nothing in its peak behavior to suggest the possibility of an echo at late epochs. The production of a light echo from such environments needs to be further explored.

The comparison of SN 2007af with other SN Ia LEs is challenging due to the multiple components. SN 1998bu is the only other clear case of a dual-feature light echo in a SN Ia, and the inner echo was also proposed to have been caused by circumstellar dust (Garnavich et al. 2001). Unfortunately, that echo and all the other SN Ia candidates were not captured with the I filter, so a rigorous comparison cannot be made. SN 2006X was the most comparable case, since it was observed in the F775W filter with *HST*. The echo from SN 2006X showed a distinct wavelength dependence, with more light scattered from shorter wavelengths. The team credits this trend to small dust size (Wang et al. 2008) This pattern is also observed in SN 2007af and can be explained with shorter wavelengths being more efficient scatterers. Since the time delay and distance to the SNe are widely different for all of the SNe cases, we are unable to make comparisons other than the ones previously stated.

5. DISCUSSION

The extended profile of the inner source, brightness, and plateau in luminosity suggest a secondary echo, but we cannot exclude the possibility of an extended source located at the SN position. A broadened FWHM does not definitively prove the existence of an inner echo, but it does eliminate the possibility of a star. However, even the bluest of stars would not replicate the $V-I$ color observed (Ducati et al. 2001). A galaxy directly behind the SN could still explain the excess emission. The FWHM analysis with local stars was performed by Wang et al. (2008) on SN 2006X, and the broadening found from that echo was only 1.10 times the local stars. Our inner echo was considerably more extended. No source (echo or other) is evident in the F160W image, which is as expected for a light echo since scattering is not efficient in the near-infrared. Also, ground-based photometry using pre-explosion subtraction images still shows an obvious flattening, making a background galaxy scenario unlikely. To confirm a secondary echo, more observations must be taken by *HST*.

The limiting magnitude of the F160W filter from the WFC3 Instrumental Handbook for a one hour exposure is 26.6 mag (Dressel 2012). Thus, an object must be fainter than this value in IR to explain the source.

The light echo color for the inner echo is roughly consistent with forward-scattered light off ISM dust, but other scattering angles cannot be eliminated. From our results, we cannot determine whether the inner echo is ISM or CSM in origin, so we will outline the arguments from both sides.

At early epochs, the Na D absorption showed no variation, providing no supporting evidence of CSM material. If the inner echo is of circumstellar origin with the scattering material located behind the SN, the same line variance as seen in SN 2006X would not be observed. Blondin et al. (2009) reported the second case of variable Na I D lines from SN 1999cl. SN 1999cl and SN 2006X were the two most reddened objects in the sample, suggesting the possible relation between high amounts of reddening and time-variable lines. Perhaps the low-reddening of SN 2007af produced a weaker Na D line, which would be more difficult to detect or, as the paper suggests, there exists a preferred line of sight to observe the spectral line variability.

The upper limit distance derived between the SN and the dust is ~90 pc, which suggests an ISM origin of the inner echo. SN 2006X and SN 1998bu have LEs that have been argued to come from the circumstellar environment, but both have distances to the dust well inside our value (<10 pc for SN 1998bu (Cappellaro et al. 2001; Garnavich et al. 2001)). Further investigation is necessary to explain how the inner and outer echoes created from ISM dust sheets could produce different colors.

Abnormal dust should be considered in the case of these echoes. Goobar (2008) argues that CSM dust around SNe Ia lowers R_V values due to multiple scattering of photons, which could explain the different color seen between the inner and outer echoes. CSM dust could also be the reason why the inner echo color is slightly bluer than the backscattering predictions.

A CSM echo suggests the SD nature of the progenitor system. However, Patat et al. (2006) argue that the existence of CSM around SNe Ia requires the dust to be optically thick, which is not what was found in our analysis. The reason for this is that the dust near the SN might be destroyed by the original SN flux, making a circumstellar echo unlikely. However, the CSM can be arbitrarily thick if backscattered, and therefore, not on the line of sight.

6. CONCLUSIONS

We present the two-component light echo discovery from SN 2007af in NGC 5584 detected in sequenced images from *HST* three years after explosion. Out of the four filters utilized in the Cepheid campaign, three show the ring-like structure of an outer echo and extended central inner echo component. Ground-based observations taken at the same epoch also show the same uncharacteristic late brightness of the normal SN Ia that remains constant, which is attributed to the presence of a light echo. Our observations in the nebular phase, where the light from the SN has faded sufficiently enough to let the light echo dominate the emission, are vital for probing the SN environment.

Using the difference between the extinction-corrected peak magnitude and echo magnitude, the optical depth of the dust was estimated, showing the optically thin nature of both dust sheets. The total magnitude difference (~11.3 mag in V) was consistent with reddening values inferred from the peak. By using the Patat (2005) model, the collection of SN Ia LEs was well-approximated. SN 2007af fit the single scattering approximation of this model.

The outer echo F350LP magnitude was found to be ~24.6 mag, ~24.6 mag in F555W, and the F814W magnitude was ~25.0 mag. The average distance from the SN to the dust sheet that created the outer echo was 790 ± 60 pc. The dust color was not consistent with Galactic dust in the forward-scattering scenario. The color was better replicated by back-scattering, but the inefficiency in that scattering method suggests abnormal dust. The brighter outer echo compared to the inner echo suggests that the outer echo dust sheet dominates the extinction in the SN peak light curves.

The inner echo of SN 2007af is the best imaged candidate for a CSM echo. Even though the Simon et al. (2007) publication saw no significant evidence of CSM using high- and low-resolution spectroscopy, they do note that there could be a preferred geometry for observing the time-variance in spectral lines. The FWHM of the inner echo was 1.5 times broader than the field stars, illustrating the extended nature of the central component and confirming that the source was not a star at the location of the SN. No galactic source was found at the location of the IE in the F160W image, supporting the argument of a secondary echo. The inner echo magnitude in the F350LP filter was ∼25.3, ∼25.2 mag in F555W, and ∼26.1 mag in F814W. The average SN to dust distance was estimated to be 90 ± 20 pc for a dust sheet located in front of the SN. For a dust sheet located directly behind the SN, a distance of 0.45 ± 0.01 pc was determined. Although the inner echo color was consistent with forward scattering, backscattering could not be eliminated, and the color was quite different from the outer echo, suggesting that even lower total-to-selective extinction ratios, other geometries, or atypical dust must be considered.

REFERENCES

Bessell, M. S. 2005, ARA&A, 43, 293
Blondin, S., Prieto, J. L., Patat, F., et al. 2009, ApJ, 693, 207
Bond, H. E., Henden, A., Levay, Z. G., et al. 2003, Natur, 422, 405
Cappellaro, E., Patat, F., Mazzali, P. A., et al. 2001, ApJL, 549, L215
Couderc, P. 1939, AnAp, 2, 271
Crotts, A. 2014, arXiv:1409.8671
Crotts, A. P. S. 1988, ApJL, 333, L51
Crotts, A. P. S., & Yourdon, D. 2008, ApJ, 689, 1186
Draine, B. T. 2003, ApJ, 598, 1017
Dressel, L. 2012, Wide Field Camera 3 Instrument Handbook HST, ed. L. Dressel (Baltimore, MD: STScI)
Ducati, J. R., Bevilacqua, C. M., Rembold, S. B., & Ribeiro, D. 2001, ApJ, 558, 309
Garnavich, P. M., Kirshner, R. P., Challis, P., et al. 2001, BAAS, 33, 1370
Goobar, A. 2008, ApJL, 686, L103
Gouiffes, C., Rosa, M., Melnick, J., et al. 1988, A&A, 198, L9
Havlen, R. J. 1972, A&A, 16, 252
Hicken, M., Challis, P., Jha, S., et al. 2009, ApJ, 700, 331
Howell, D. A. 2001, ApJL, 554, L193
Humphreys, E. M. L., Reid, M. J., Moran, J. M., Greenhill, L. J., & Argon, A. L. 2013, ApJ, 775, 13
Kankare, E., Fraser, M., Ryder, S., et al. 2014, A&A, 572, A75
Koribalski, B. S., Staveley-Smith, L., Kilborn, V. A., et al. 2004, AJ, 128, 16
Krause, O., Tanaka, M., Usuda, T., et al. 2008, Natur, 456, 617
Landolt, A. U. 1992, AJ, 104, 340
Liu, J.-F., Bregman, J. N., & Seitzer, P. 2003, ApJ, 582, 919
Maund, J. R., & Smartt, S. J. 2005, MNRAS, 360, 288
Miller, A. A., Smith, N., Li, W., et al. 2010, AJ, 139, 2218
Milne, P. A., The, L.-S., & Leising , M. D. 1999, ApJS, 124, 503
Moore, K., & Bildsten, L. 2012, ApJ, 761, 182
Nobili, S., & Goobar, A. 2008, A&A, 487, 19
Nugent, P., Kim, A., & Perlmutter, S. 2002, PASP, 114, 803
Ortiz, J. L., Sugerman, B. E. K., de La Cueva, I., et al. 2010, A&A, 519, A7
Otsuka, M., Meixner, M., Panagia, N., et al. 2012, ApJ, 744, 26
Panagia, N., Gilmozzi, R., Macchetto, F., Adorf, H.-M., & Kirshner, R. P. 1991, ApJL, 380, L23
Patat, F. 2005, MNRAS, 357, 1161
Patat, F., Benetti, S., Cappellaro, E., & Turatto, M. 2006, MNRAS, 369, 1949
Patat, F., Chandra, P., Chevalier, R., et al. 2007, Sci, 317, 924
Quinn, J. L., Garnavich, P. M., Li, W., et al. 2006, ApJ, 652, 512
Raskin, C., & Kasen, D. 2013, ApJ, 772, 1
Rest, A., Matheson, T., Blondin, S., et al. 2008, ApJ, 680, 1137
Riess, A. G., Macri, L., Casertano, S., et al. 2011, ApJ, 730, 119
Ritchey, G. W. 1901a, ApJ, 14, 293
Ritchey, G. W. 1901b, ApJ, 14, 167
Ritchey, G. W. 1902, ApJ, 15, 129
Salgado, F., Hamuy, M., Morrell, N., & Folatelli, G. 2007, CBET, 865, 1
Schmidt, B. P., Kirshner, R. P., Leibundgut, B., et al. 1994, ApJL, 434, L19
Shen, K. J., Bildsten, L., Kasen, D., & Quataert, E. 2012, ApJ, 748, 35
Simon, J. D., Gal-Yam, A., Penprase, B. E., et al. 2007, ApJL, 671, L25
Sparks, W. B. 1994, ApJ, 433, 19
Sugerman, B. E. K. 2003, AJ, 126, 1939
Sugerman, B. E. K. 2005, ApJL, 632, L17
Sugerman, B. E. K., Andrews, J. E., Barlow, M. J., et al. 2012, ApJ, 749, 170
Suntzeff, N. B. 1996, in IAU Colloq 145, Supernovae and Supernova Remnants ed. R. McCray, & Z. Wang, 41
Suntzeff, N. B., Heathcote, S., Weller, W. G., Caldwell, N., & Huchra, J. P. 1988, Natur, 334, 135
Swope, H. H. 1940, BHarO, 913, 11
Tody, D. 1986, in Proc SPIE, 627, 733
van Dyk, S. D. 2013, ApJ, 146, 24
van Dyk, S. D., Li, W., & Filippenko, A. V. 2003, PASP, 115, 1
Wang, L. 2005, ApJL, 635, L33
Wang, X., Li, W., Filippenko, A. V., et al. 2008, ApJ, 677, 1060